Applied Physics Letters

Metal-insulator transition of $SrVO_3$ ultrathin films embedded in $SrVO_3/SrTiO_3$ superlattices

Cite as: Appl. Phys. Lett. **117**, 133105 (2020); https://doi.org/10.1063/5.0020615
Submitted: 02 July 2020 . Accepted: 12 September 2020 . Published Online: 29 September 2020

Jun Wang, Nicolas Gauquelin, Mark Huijben, Jo Verbeeck, Guus Rijnders, and Gertjan Koster

Applied Physics Letters ARTICLE scitation.org/journal/apl

Metal-insulator transition of $SrVO_3$ ultrathin films embedded in $SrVO_3/SrTiO_3$ superlattices

Cite as: Appl. Phys. Lett. **117**, 133105 (2020); doi: 10.1063/5.0020615
Submitted: 2 July 2020 · Accepted: 12 September 2020 ·
Published Online: 29 September 2020

Jun Wang,[1] Nicolas Gauquelin,[2] Mark Huijben,[1] Jo Verbeeck,[2] Guus Rijnders,[1] and Gertjan Koster[1,a)]

AFFILIATIONS

[1]Faculty of Science and Technology and MESA+ Institute for Nanotechnology, University of Twente,7500 AE Enschede, The Netherlands
[2]Electron Microscopy for Materials Science (EMAT), University of Antwerp, 2020 Antwerp, Belgium

[a)]Author to whom correspondence should be addressed: g.koster@utwente.nl

ABSTRACT

The metal-insulator transition (MIT) in strongly correlated oxides is a topic of great interest for its potential applications, such as Mott field effect transistors and sensors. We report that the MIT in high quality epitaxial $SrVO_3$ (SVO) thin films is present as the film thickness is reduced, lowering the dimensionality of the system, and electron-electron correlations start to become the dominant interactions. The critical thickness of 3 u.c is achieved by avoiding effects due to off-stoichiometry using optimal growth conditions and excluding any surface effects by a STO capping layer. Compared to the single SVO thin films, conductivity enhancement in SVO/STO superlattices is observed. This can be explained by the interlayer coupling effect between SVO sublayers in the superlattices. Magnetoresistance and Hall measurements indicate that the dominant driving force of MIT is the electron–electron interaction.

Transition metal oxides are an interesting and important class of functional materials. The complex interplay between the spin, charge, and orbital generates a broad range of electrical and magnetic properties.[1,2] Physical properties can be tuned by introducing the interface, surface, strain, and reduced dimensionality.[3–6] The well-known system, $LaAlO_3/SrTiO_3$, exhibits a two dimensional electron gas with high mobility at the interface between two band-insulators.[7] Many metallic oxides, such as $SrRuO_3$ and $LaSrMnO_3$, become non-metallic when they are confined below a critical thickness. The metal-insulator transition (MIT) in strongly correlated oxides has received a lot of interest because of its potential to be used for electronic devices, such as Mott field effect transistors and sensors.[8]

$SrVO_3$ (SVO) with a $3d^1$ electronic configuration for vanadium is a model strongly correlated system for the study of the MIT.[9,10] According to the Mott–Hubbard theory, the two controllable parameters for a Mott transition are filling control and bandwidth control.[1] One of the approaches to control the bandwidth is by reducing the thickness of the films. Ultrathin SVO films were previously studied by *in situ* photoemission spectroscopy (PES), showing the evolution of the electronic structure of SVO thin films.[11] A Mott–Hubbard bandgap opened at the Fermi level for the film with a thickness of 2–3 unit cells (u.c). Therefore, the authors concluded that the insulating state was driven by the reduction of the bandwidth due to a dimensional crossover. More recent works studied the dimensional crossover MIT of SVO ultrathin films by *ex situ* transport measurements. The MIT occurred at 200 K for films grown with a thickness of 3 nm by Gu *et al.*,[12] while Fouchet *et al.* found insulating behavior in the temperature range from 2 K to 300 K for a film with a thickness of 2 nm.[13] The critical thicknesses determined by the transport measurement are typically higher than those concluded from the *in situ* study of the evolution of the electronic structure. In another system, Liao *et al.*[6] showed that extrinsic factors, such as oxygen vacancies, enhance the nonmetallic behavior in LSMO thin films. It was reported that the critical thickness of thin films grown at low oxygen pressures was higher than that of thin films grown at high oxygen pressures. Moreover, they showed that a capping layer can be used to improve the metallic behavior in ultrathin films by minimizing any effective surface off-stoichiometry.

Therefore, to gain more insight into the origin of the MIT of SVO thin films, it is important to precisely control the thickness of the films and to minimize extrinsic factors. In previous *ex situ* studies, the thickness of the SVO thin film is not so well defined in units of unit cells and the thin films are not capped. While in this work, the thickness of SVO thin films was controlled at the sub-unit cell level by monitoring the reflection high-energy electron diffraction (RHEED) intensity oscillations during growth. Furthermore, a $SrTiO_3$ (STO)

capping layer was introduced. Next to reducing the thickness of single thin films, the dimensional crossover-driven MIT was studied in the ultrathin layers embedded in superlattices. Typically, a superlattice can be used to understand the properties that are present in a single low dimensional system because the properties of a single period can be enhanced due to periodic repetition. However, depending on the sublayer thicknesses used, the properties of superlattices differ from a single layer system. Although Sun *et al.*[14] showed conductivity enhancement of ultrathin $LaNiO_3$ films in superlattices, the interlayer coupling between each adjacent sublayer in the superlattice is still an open question. Here, we study and compare both ultrathin SVO layers with a STO capping layer as well as STO/SVO superlattices in order to understand the interlayer coupling effect between the metallic sublayers.

SVO thin films were grown by pulsed laser deposition equipped with RHEED. Our previous study[15] showed that the stoichiometry of SVO thin films was controlled by carefully selecting proper argon and oxygen partial pressures. The partial oxygen pressure of 1×10^{-5} mbar with the background argon pressure of 0.025 mbar is the optimal condition to ensure prefect Sr:V = 1:1 stoichiometry. To minimize any stoichiometry effects on the metal-insulator transition, all SVO thin films were grown at these conditions. To avoid the over-oxidation of the SVO layer, the STO layer was also grown at the same pressure. A thermal and chemical treatment was applied to achieve single TiO_2 terminated $SrTiO_3$ (100) (STO) substrates.[16] The substrate temperature was set at 600 °C by laser heating. For ablation, a 248 nm wavelength KrF excimer laser was employed with a fluence of 2 J/cm^2 set at a repetition rate of 1 Hz. The fluence of 2 J/cm^2 used for the STO layer can compensate the off-stoichiometry of STO thin films caused by the low oxygen partial pressure.[17] During the growth, the intensity of a specular spot in a RHEED pattern was monitored. For the 2D nucleation and growth, oscillations of the RHEED intensity are related to the periodic formation of growing islands, giving alternating step density. Therefore, one oscillation period corresponds to the deposition time of approximately one unit cell in the case of layer-by-layer growth, which was used to determine the thickness of thin films. First, capped SVO thin films were grown. The thickness of the SVO layer was varied from 3 u.c to 6 u.c. The 2 u.c thick STO layer was used to cap all SVO films. Next, in order to understand the coupling effect between metallic sublayers, superlattices $[(SVO)_m/(STO)_2]_{10}(2 \le m \le 4)$ and $[(SVO)_4/(STO)_n]_{10}(1 \le n \le 3)$ were also grown.

The surface morphology of the grown films was investigated by atomic force microscopy (Bruker AFM) in a tapping mode. X-ray diffraction (XRD) was used to characterize the crystal structure of SVO/STO superlattices (Xpert panalytical MRD). Although the ultrathin SVO layer is too thin to be seen in the XRD measurement, the crystal structure can be determined by RHEED. In addition to the XRD measurement, the structural and chemical properties of the superlattice $[(SVO)_2/(STO)_2]_{10}$ were visualized by Cs-corrected scanning transmission electron microscopy (STEM) equipped with a Gatan Enfina spectrometer for Electron Energy Loss Spectroscopy (EELS). The microscope was operated at 300 kV with a 20 mrad convergence angle. The transport properties of all the samples were measured by a Physical Properties Measurement System (PPMS) using the van der Pauw method in the 2 K–300 K temperature range. Hall and magnetoresistance (MR) measurements were performed in a perpendicular magnetic field from −9 T to 9 T to understand the driving force behind the MIT.

The tapping mode AFM image of the 6 u.c capped $SrVO_3$ thin film is shown in Fig. S1(a). The smooth surface with the step-terrace structure is observed. The RHEED specular spot intensity vs time [Fig. S1(b)] shows six oscillations, which indicates that the thickness of the SVO is 6 u.c. Although the capped SVO thin films are too thin to be observed in the XRD measurement, the RHEED pattern shown in Fig. S1(a) can indicate that capped SVO samples are epitaxial grown and have high crystallinity. XRD 00l scans around the (002) Bragg reflection of superlattices $[(SVO)_m/(STO)_2]_{10}(2 \le m \le 4)$ and $[(SVO)_4/(STO)_n]_{10}(1 \le n \le 3)$ are shown in 1(a) and 1(b), respectively. In Fig. 1(a), the zeroth-order superlattice peak, which is close to the STO substrate peak, is observed for all superlattices. The averaged out-of-plane lattice constant derived from the superlattice peak decreases with the increasing thickness of SVO sublayers. The Laue fringes around the superlattice peaks originating from the coherence between individual sublayers indicate smooth interfaces between the SVO and STO layers. The first-order satellite peaks indicate that a long-range order is present in the superlattices $[(SVO)_3/(STO)_2]_{10}$ and $[(SVO)_4/(STO)_2]_{10}$. The thickness of the SVO/STO bilayer can be estimated from the angular distance between the superlattice peak and the satellite peak. Since the atomic size of vanadium and titanium is similar, the contrast between SVO and STO is very weak. The intensity of first-order satellite peaks for the $[(SVO)_2/(STO)_2]_{10}$ superlattice is too low to be observed. This low contrast also causes that the SVO and STO are hardly distinguishable in the TEM image of superlattice $[(SVO)_2/(STO)_2]_{10}$ [Fig. 1(c)]. This TEM image shows the high crystallinity of the superlattice $[(SVO)_2/(STO)_2]_{10}$. Chemical maps obtained by EELS of the Ti $L_{2,3}$ and V $L_{2,3}$ for the region in the rectangle of the TEM image are also shown in Fig. 1(c), demonstrating atomically sharp ordered SVO/STO interfaces. This also shows that

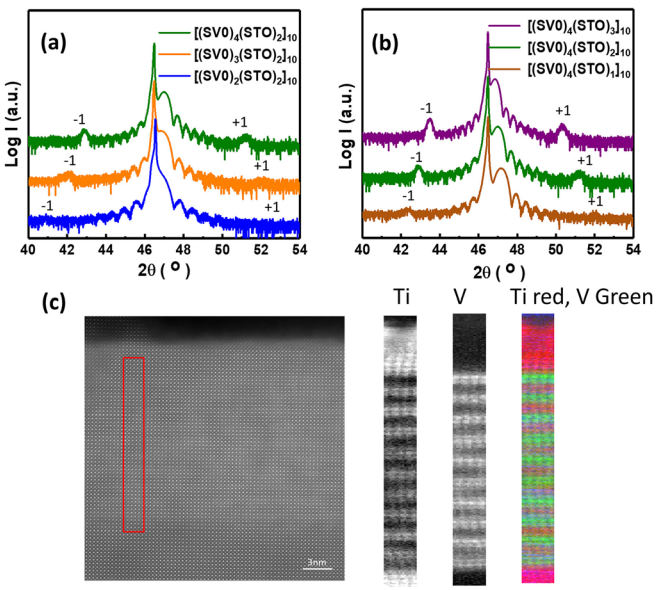

FIG. 1. (a) XRD 00l scans around (002) Bragg reflection of (a) $[(SVO)_m/(STO)_2]_{10}(2 \le m \le 4)$ and (b) $[(SVO)_4/(STO)_n]_{10}(1 \le n \le 3)$. (c) TEM image at low magnification showing the superlattice $[(SVO)_2/(STO)_2]_{10}$ structure and chemical maps obtained by EELS of the Ti $L_{2,3}$ and V $L_{2,3}$ for the region in the red rectangle of the TEM image.

there is no perceptible atomic inter-diffusion at the interface between SVO and STO. The valence analysis of Ti $L_{2,3}$ edge is shown in Fig. S2. The sign of Ti^{4+} for each STO sublayer indicates that STO sublayers in the superlattice are stoichiometric without oxygen vacancies. In Fig. 1(b), the zeroth-order superlattice peak is clearly seen for all superlattices. The averaged out-of-plane lattice constant derived from the superlattice peaks increases with increasing the thickness of STO sublayers. Again, the Laue fringes around the superlattice peaks indicate smooth interfaces between the SVO and STO layers. The first-order satellite peak becomes sharper as the number of STO sublayers increases from 1 to 3 u.c.

The electrical resistivity as a function of temperature ranging from 2 K to 300 K for a single capped SVO system is shown in Fig. 2(a). The thickness of the SVO layer varies from 3 u.c to 6 u.c. A thick SVO film, as shown in Fig. S3 in the supplementary material, shows metallic behavior: the resistivity decreases with a decrease in the temperature. The electricity resistivity as a function of temperature can be expressed by $\rho = \rho_0 + AT^2$, where the residual resistivity ρ_0 is temperature independent, attributed to the electron-impurity scattering. The coefficient A quantifies the electron–electron interaction relation. This dependence corresponds to the Fermi liquid behavior in correlated electrons. The resistivity of SVO thin films with a reduced thickness in Fig. 2(a) is higher compared to that of the thick SVO film. The upturn occurs in the curve for SVO ultrathin films with the thickness below 6 u.c. In the metallic regime, the temperature dependence of resistivity still follows the T^2 law (dashed line in Fig. 2). The residual resistivity ρ_0 and coefficient A for these films are shown in Table S1. The transition temperature (T_{MIT}) for each film, as indicated by a black arrow in Fig. 2(a), is defined by the peak position at the $d\rho/dT$ curve. T_{MIT} is 42 K for the 6 u.c capped film and then increases to 100 K for the 4 u.c capped film. The critical thickness of SVO is 3 u.c at which the insulating behavior presents in the whole temperature range. Mott suggested the minimum metallic value $\sigma_M = C_{Me}^2/\hbar n_c^{-1/3}$, where $C_M = 1/20$ and n_c is the carrier concentration.[18] The Hall measurement shows that the carrier concentration of our SVO thin films is about 1×10^{22} cm^{-3}. The minimum metallic value calculated from the equation is 42 $(\Omega\,\mathrm{cm})^{-1}$. Therefore, the Mott minimum resistivity of SVO is $2.4 \times 10^{-2}\,\Omega$ cm. Although the resistivity of 3 u.c SVO at low temperature is out of the measurement limit in our equipment, we expect that its resistivity is of the same order of the calculated minimum resistivity at low temperature. Mott, Ioffe, and Regel later pointed out that the metallic state cannot survive if the mean free path l is larger than interatomic spacing or k_F^{-1}, k_F being the Fermi wave number. When $k_F l$ is close to one, the MIT is expected. For a 2D system, the Mott–Ioffe–Regel (MIR) limit is related to sheet resistance (R_{sheet}) of 25 KΩ. The sheet resistance of the 3 u.c capped SVO thin film is 22 KΩ at room temperature, which is the same order of the MIR limit. This critical thickness agrees well with the thickness measured by *in situ* photoemission spectroscopy (PES),[12] whereas this is lower than the critical thickness studied by transport measurement in the literature.[13,14] These transport properties of capped SVO indicate that our SVO films are close to stoichiometry and surface effects also play a role.

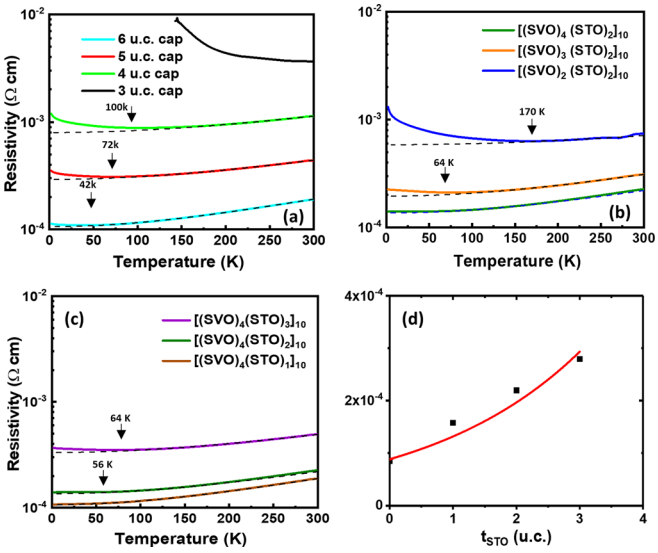

FIG. 2. (a) Temperature-dependent resistivity for films with different thicknesses in the range from 3 u.c to 6 u.c All the SVO films were capped by a 2 u.c layer. The metal-insulator transition temperatures are indicated by a black arrow. The resistivity as a function of temperature for (b) $[(SVO)_m/(STO)_2]_{10}(2 \le m \le 4)$ and (c) $[(SVO)_4/(STO)_n]_{10}(1 \le n \le 3)$ superlattices. The metal-insulator transition temperature is also indicated by a black arrow. The dashed line shows the fitting of $\rho = \rho_0 + AT^2$ for each film. (d) Resistivity of superlattices ρ as a function of the thickness of STO sublayer t_{STO}. The data are fitted to $\rho = \rho_0 e^{t_{STO}/2.48}$ shown in a red solid line.

The temperature-dependent resistivity in the range from 2 K to 300 K of the superlattices is shown in Figs. 2(b) and 2(c). Strikingly, the transport properties of the superlattice $[(SVO)_4/(STO)_2]_{10}$ are not the same as the single 4 u.c capped SVO system. The conductivity of this superlattice is enhanced [Fig. 2(b)], and the metallic behavior is present in the whole temperature range. The conductivity can be further improved by reducing the thickness of STO sublayers to 1 u.c between the SVO sublayers [Fig. 2(c)]. However, the MIT occurs at 64 K in the superlattice $[(SVO)_4/(STO)_3]_{10}$ [Fig. 2(c)] and also occurs with further reducing the SVO thickness in SVO/STO superlattices. In Fig. 2(b), T_{MIT} is 64 K for the superlattice $[(SVO)_3/(STO)_2]_{10}$ and 170 K for the superlattice $[(SVO)_2/(STO)_2]_{10}$. Again, the temperature dependence of resistivity in the metallic regime still follows the T^2 law.

The conductivity enhancement in SVO/STO superlattices indicates that the interlayer coupling between the SVO sublayers plays a role. STO can be regarded as a barrier, while the current between SVO sublayers passes through the STO barriers if the thickness of STO is sufficiently low to allow for tunneling. This tunneling current would be suppressed by increasing the barrier thickness. In Fig. 2(c), the conductivity increases with the increasing thickness of the STO sublayers in the superlattices. Although the resistivity of the superlattice $[(SVO)_4/(STO)_3]_{10}$ is still lower than that of the single 4 u.c capped SVO system, the MIT behaves similarly to the capped SVO system. Figure 2(d) shows the resistivity of the superlattices ρ as a function of the thickness of STO sublayer t_{STO}. The relationship between resistivity and the thickness of STO sublayer can be described by $\rho = \rho_0 e^{t_{STO}/2.48}$. STO sublayers with the thickness of 6 u.c would be needed to completely suppress the coupling effect in superlattices. This result indicates that the transport properties of metal oxide ultrathin films in superlattices are different compared to those of individual layers. By reducing the dimensionality of the SVO layer in superlattices, the transport properties are tuned from a metal to a Mott-

insulator [Fig. 2(b)]. The critical thickness of SVO is reduced by the interlayer coupling effect in superlattices.

The results discussed above show that the temperature-driven MIT exists in the SVO ultrathin films and superlattices. The critical thickness of SVO can be reduced by avoiding effects due to off-stoichiometry and excluding any surface effects. It is important to understand the driving force behind the observed MIT. We first consider the weak localization in a two dimensional (2D) system,[19]

$$\sigma = s_0 + p * \frac{e^2}{\pi * h} \ln(T/T_0), \quad (1)$$

where σ is the Drude conductivity, e is the charge of the electron, h is Planck's constant, and T_0 is related to the transport mean free path. If the main inelastic relaxation mechanism is electron–electron scattering, $p = 1$, whereas electron-phonon scattering gives rise to $p = 3$. The linear behavior of the conductance as a function of ln(T) at low temperature for the capped SVO system is shown in Fig. 3. For the 6 u.c capped SVO and 5 u.c capped SVO, the calculation from Eq. (1) with the electron–electron scattering ($p = 1$) and the electron-phonon scattering ($p = 3$) cannot describe the experimental data [Figs. 3(a) and 3(b)]. For the 4 u.c capped SVO, the fitting with $p = 1$ agrees with the data at low temperature. However, the fit deviates slightly for the temperature above 30 K ($\ln T = 3.4$). The resistance of 3 u.c at low temperature is out of the measurement limit in our PPMS equipment. Therefore, we did not further analyze the 3 u.c. thick film. In a 2D model established by Lee and Ramakrishnan,[19] one point that needs to be noted is that the electron-electron interaction would also affect the logarithmic temperature dependence of the conductivity. Both of these effects can be further clarified by analyzing the magnetoresistance (MR).

In Fig. 4(a), a positive MR in a perpendicular magnetic field from −9 T to 9 T is observed for the single 4 u.c capped SVO at temperature below the transition temperature. MR at a temperature higher than 5 K is proportional to H^2, which can be attributed to a Lorentz force. The positive MR does not correspond to the weak localization because the magnetic field suppresses the coherent interference for localization, leading to a negative MR. Instead, the positive MR over the entire range is an indication of electron-electron interaction. The Hall measurement of the 4 u.c capped SVO film is shown in Fig. 4(b). This figure shows that the carriers are electrons and their density slightly decreases as the temperature decreases. The carrier mobility increases with the decreasing temperature. The values of carrier density and the carrier mobility are similar to those of a thick SVO film. The Hall coefficient was found to increase logarithmically at a rate equal to twice that of the resistivity at low temperature for the localization effect.[19] The

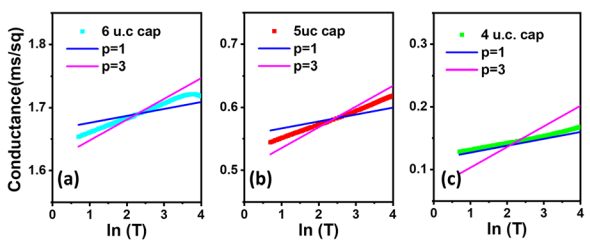

FIG. 3. Sheet conductance at low temperature is presented as a function of Ln (T) for the capped SVO systems with (a) 6 u.c SVO, (b) 5 u.c SVO, and (c) 4 u.c SVO. A 2D model for the weak localization with $p = 1$ (blue line) and $p = 3$ (purple line).

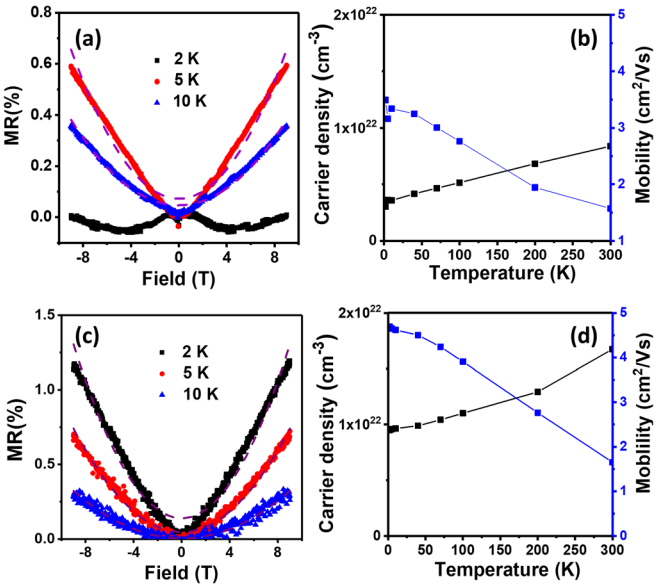

FIG. 4. Magnetoresistance in the perpendicular field for (a) the 2 u.c STO capped 4 u.c SVO film and (c) the superlattice $[(SVO)_4/(STO)_2)]_{10}$ at low temperature. The parabolic fits to the dependency of H^2 at each temperature are shown in purple dashed lines. Carrier density and mobility variation as a function of temperature for (b) the 2 u.c STO capped 4 u.c SVO film and (d) the superlattice $[(SVO)_4/(STO)_2)]_{10}$.

decrease in the carrier density with the decrease in the temperature observed here is not the dependency of the Hall coefficient for the localization. At $T = 5$ K, a quick rise in MR with a linear behavior is observed. This behavior is likely due to the weak antilocalization (WAL) effect, which originates from the destructive interference of coherently backscattered conduction electrons due to spin rotations. Interestingly, for the temperature at 2 K, a competition of negative (small H) and positive MR (large H) is observed, which shows the interplay of electron-electron interaction and weak localization. This weak localization is likely to be caused by spin fluctuations, possibly originating from the slight oxygen deficiency in our SVO thin films. The STEM spectrum analysis shown in Fig. S2 indicates that the V^{3+} is present at the interface between the first layer of SVO and STO substrates. If T is sufficiently low, some amount of magnetic fluctuations and scattering on these fluctuations by diffusing electrons could dominate orbital contributions and impact MR. This behavior was also observed and discussed in the $LaNiO_3$ ultrathin film.[5] In Fig. 4(c), MR in a perpendicular magnetic field at low temperature for the superlattice $[(SVO)_4/(STO)_2)]_{10}$ is also proportional to H^2. The positive sign indicates that the dominant driving force behind the MIT in the superlattice is electron–electron interaction as opposed to weak localization. MR measurements for the superlattices $[(SVO)_4/(STO)_1)]_{10}$ and $[(SVO)_4/(STO)_3)]_{10}$ are shown in the supplementary material. The positive MR is present for all superlattice samples. The carrier density shown in Fig. 4(d) is higher than that in the capped SVO. This also can be caused by a still finite coupling between SVO sublayers in the superlattice.

The high quality epitaxial SVO ultrathin films show a metal-insulator transition driven by the dimensionality effect. The critical thickness of 3 unit cells was achieved by suppressing the stoichiometric

effect under optimal growth conditions and excluding any surface effects by a $SrTiO_3$ (STO) capping layer. A detailed investigation of transport measurements of SVO ultrathin films indicates that the dominant driving force of MIT is the electron–electron interaction. Furthermore, epitaxial SVO/STO superlattices were fabricated. The conductivity of the SVO layer is enhanced in the superlattice compared to that of the capped SVO. This behavior can be interpreted as the interlayer coupling between SVO sublayers in the superlattice. The coupling effect can be suppressed by increasing the thickness of the STO barrier layers in the superlattice.

See the supplementary material for the AFM image of a 2 u.c STO capping layer on the 6 u.c $SrVO_3$ thin film; EELS fine structure of Ti $L_{2,3}$ in top layers of each STO sublayer and bottom layers of each STO sublayer and V $L_{2,3}$ in top layers of each SVO sublayer and bottom layers of each SVO sublayer in the supperlattice; temperature-dependent resistivity of the film with a thickness of 80 u.c; overview of electrical properties for capped SVO systems; and SVO/STO superlattices and magnetoresistance measurements for 5 u.c capped, 6 u.c capped, $[(SVO)_4/(STO)_1)]_{10}$, $[(SVO)_4/(STO)_3)]_{10}$, $[(SVO)_2/(STO)_2)]_{10}$, and $[(SVO)_2/(STO)_2)]_{10}$ samples.

We thank Alexander Brinkman for valuable discussions. This work was supported by Nederlandse Organisatie voor Wetenschappelijk Onderzoek through Grant No. 13HTSM01.

DATA AVAILABILITY

The data that support the findings of this study are available from the corresponding author upon reasonable request.

REFERENCES

[1]M. Imada, A. Fujimori, and Y. Tokura, Rev. Mod. Phys. **70**, 1039 (1998).
[2]I. H. Inoue and M. J. Rozenberg, Adv. Funct. Mater. **18**, 2289 (2008).
[3]H. Y. Hwang, Y. Iwasa, M. Kawasaki, B. Keimer, N. Nagaosa, and Y. Tokura, Nat. Mater. **11**, 103 (2012).
[4]D. G. Schlom, L.-Q. Chen, C.-B. Eom, K. M. Rabe, S. K. Streiffer, and J.-M. Triscone, Annu. Rev. Mater. Res. **37**, 589 (2007).
[5]R. Scherwitzl, S. Gariglio, M. Gabay, P. Zubko, M. Gibert, and J.-M. Triscone, Phys. Rev. Lett. **106**, 246403 (2011).
[6]Z. Liao, F. Li, P. Gao, L. Li, J. Guo, X. Pan, R. Jin, E. Plummer, and J. Zhang, Phys. Rev. B **92**, 125123 (2015).
[7]A. Ohtomo and H. Hwang, Nature **427**, 423 (2004).
[8]Z. Yang, C. Ko, and S. Ramanathan, Annu. Rev. Mater. Res. **41**, 337 (2011).
[9]Y. Lan, X. Chen, and M. He, J. Alloys Compd. **354**, 95 (2003).
[10]J. A. Moyer, C. Eaton, and R. Engel-Herbert, Adv. Mater. **25**, 3578 (2013).
[11]K. Yoshimatsu, T. Okabe, H. Kumigashira, S. Okamoto, S. Aizaki, A. Fujimori, and M. Oshima, Phys. Rev. Lett. **104**, 147601 (2010).
[12]M. Gu, S. A. Wolf, and J. Lu, Adv. Mater. Interfaces **1**, 1300126 (2014).
[13]A. Fouchet, M. Allain, B. Bérini, E. Popova, P.-E. Janolin, N. Guiblin, E. Chikoidze, J. Scola, D. Hrabovsky, Y. Dumont *et al.*, Mater. Sci. Eng., B **212**, 7 (2016).
[14]J. Son, J. M. LeBeau, S. J. Allen, and S. Stemmer, Appl. Phys. Lett. **97**, 202109 (2010).
[15]J. Wang, G. Rijnders, and G. Koster, Appl. Phys. Lett. **113**, 223103 (2018).
[16]G. Koster, B. L. Kropman, G. J. H. M. Rijnders, D. H. A. Blank, and H. Rogalla, Appl. Phys. Lett. **73**, 2920 (1998).
[17]R. Groenen, J. Smit, K. Orsel, A. Vailionis, B. Bastiaens, M. Huijben, K. Boller, G. Rijnders, and G. Koster, APL Mater. **3**, 070701 (2015).
[18]M. A. Paalanen, T. F. Rosenbaum, G. A. Thomas, and R. N. Bhatt, Phys. Rev. Lett. **48**, 1284 (1982).
[19]P. A. Lee and T. Ramakrishnan, Rev. Mod. Phys. **57**, 287 (1985).